Protein Structure and Folding:

Structural and Biochemical Analyses of the Eukaryotic Heat Shock Locus V (HslV) from *Trypanosoma brucei*

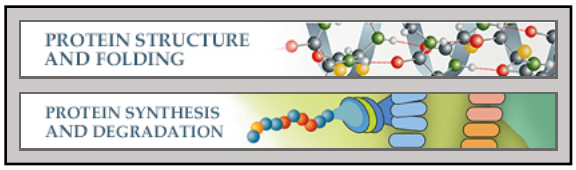

Kwang Hoon Sung, So Yeon Lee and Hyun Kyu Song

J. Biol. Chem. 2013, 288:23234-23243.
doi: 10.1074/jbc.M113.484832 originally published online July 1, 2013

THE JOURNAL OF BIOLOGICAL CHEMISTRY VOL. 288, NO. 32, pp. 23234–23243, August 9, 2013

Structural and Biochemical Analyses of the Eukaryotic Heat Shock Locus V (HslV) from *Trypanosoma brucei*[*]

Received for publication, May 20, 2013, and in revised form, June 21, 2013 Published, JBC Papers in Press, July 1, 2013, DOI 10.1074/jbc.M113.484832

Kwang Hoon Sung, So Yeon Lee, and Hyun Kyu Song[1]

From the Department of Life Sciences, Korea University, Anam-Dong, Seongbuk-Gu, Seoul 136-701, Korea

Background: A eukaryotic HslV (TbHslV) protease and two potential HslU (TbHslU1 and TbHslU2) ATPases have been isolated from *Trypanosoma brucei*.
Results: We determined the crystal structure of TbHslV at 2.4 Å resolution. Only TbHslU2 activated TbHslV protease activity.
Conclusion: A key tyrosine residue in TbHslU2 required for activating TbHslV was identified.
Significance: This study lays the groundwork for understanding the eukaryotic HslVU system.

In many bacteria, heat shock locus V (HslV) functions as a protease, which is activated by heat shock locus U (HslU). The primary sequence and structure of HslV are well conserved with those of the β-subunit of the 20 S proteasome core particle in eukaryotes. To date, the HslVU complex has only been characterized in the prokaryotic system. Recently, however, the coexistence of a 20 S proteasome with HslV protease in the same living organism has been reported. In *Trypanosoma brucei*, a protozoan parasite that causes human sleeping sickness in Africa, HslV is localized in the mitochondria, where it has a novel function in regulating mitochondrial DNA replication. Although the prokaryotic HslVU system has been studied extensively, little is known regarding its eukaryotic counterpart. Here, we report the biochemical characteristics of an HslVU complex from *T. brucei*. In contrast to the prokaryotic system, *T. brucei* possesses two potential HslU molecules, and we found that only one of them activates HslV. A key activating residue, Tyr^{494}, was identified in HslU2 by biochemical and mutational studies. Furthermore, to our knowledge, this study is the first to report the crystal structure of a eukaryotic HslV, determined at 2.4 Å resolution. Drawing on our comparison of the biochemical and structural data, we discuss herein the differences and similarities between eukaryotic and prokaryotic HslVs.

In prokaryotes, two-component ATP-dependent proteases, such as HslVU,[2] ClpAP, and ClpXP, act as protein quality controllers via destruction and recycling of misfolded or damaged proteins (1). In the ATP-dependent proteases, the ATPase unfolds and translocates substrates, whereas the protease degrades the unfolded substrate. The protein degradation mechanism of a large eukaryotic protease complex, termed the 26 S proteasome, is similar to that of prokaryotic ATP-dependent proteases (1–3).

The heat shock protein complex, HslVU, is a simple homolog of the eukaryotic proteasome (4, 5). In many bacteria, heat shock locus V (HslV) functions as a protease with its activator heat shock locus U (HslU), which is an unfoldase driven by ATP hydrolysis. According to MEROPS classification (see the MEROPS Web site), both HslV and the proteasome contain an N-terminal threonine that acts as the essential catalytic residue (6). They share ~20% primary sequence similarity, and the structure of HslV is well conserved with that of the β-subunit of the eukaryotic 20 S proteasome core particle (7). The dodecameric HslV, which resembles a "double donut" shape, forms a functional HslVU complex with two hexameric HslU molecules to seal the substrate entrance pores at both ends (4). The extensive biochemical study performed on the HslVU complex has rendered it a suitable model system that can be used to understand the eukaryotic 26 S proteasome (4, 5, 8–14). Until recently, the structures of the individual components HslU and HslV as well as the HslVU complex have been studied in bacteria and archaea (7, 15–22).

Although the HslVU has been detected in many prokaryotic systems, the coexistence of a proteasome with HslVU in a wide range of eukaryotic systems has recently been suggested (23–25). Among them, the HslVU from the protozoan parasites, *Leishmania*, *Trypanosoma*, and *Plasmodium*, which cause significant human diseases, including African sleeping sickness, malaria, and leishmaniasis, have been experimentally characterized (26–29). Intriguingly, HslU and HslV are localized in the mitochondria in *Trypanosoma brucei*, where they have a novel function in regulating mitochondrial DNA replication (28). The amino acid sequence of HslV from *T. brucei* (TbHslV) shares more than 40% identity with that of HslV from *Escherichia coli* (EcHslV; Fig. 1*A*). There are two potential HslU molecules, HslU1 and HslU2, in *T. brucei* (TbHslU1 and TbHslU2) that have high identity with the HslU from *E. coli* (EcHslU; Fig. 1*B*) (28).

* This work was supported by a National Research Foundation of Korea (NRF) grant funded by the Korean government (MEST) (Grant 2011-0028168) and the Korea Healthcare Technology R&D Project, Ministry for Health, Welfare, and Family Affairs, Republic of Korea (Grant A092006).
The atomic coordinates and structure factors (codes 4HNZ and 4HO7) have been deposited in the Protein Data Bank (http://wwpdb.org/).
[1] To whom correspondence should be addressed: Department of Life Sciences, Korea University, Anam-Dong, Seongbuk-Gu, Seoul 136-701, Korea. Tel.: 82-2-3290-3457; Fax: 82-2-3290-3628; E-mail: hksong@korea.ac.kr.
[2] The abbreviations used are: HslV, heat shock locus V; HslU, heat shock locus U; EcHslU, HslU from *E. coli*; $EcHslU_{TbHslU2}$, EcHslU containing C-terminal sequence of TbHslU2 segment; EcHslV, HslV from *E. coli*; HiHslU, HslU from *H. influenza*; HiHslV, HslV from *H. influenza*; MBP, maltose-binding protein; r.m.s., root mean square; TbHslU, HslU from *T. brucei*; TbHslV, HslV from *T. brucei*; TmHslV, HslV from *T. maritima*; Z, benzyloxycarbonyl; AMC, 7-amido-4-methyl coumarin.

In order to understand the molecular features of the eukaryotic HslVU system, we performed biochemical characterization of TbHslV and TbHslU by using a synthetic substrate, benzyloxycarbonyl-Gly-Gly-Leu-7-amido-4-methyl coumarin (Z-GGL-AMC) (4, 30) and a natural substrate of EcHslU, the SulA protein (31, 32). Although both TbHslU1 and TbHslU2 regulate mitochondrial DNA replication (28), we found that only TbHslU2 acts as an activator of TbHslV protease. We also determined the first structure of the eukaryotic TbHslV. The general structural features of eukaryotic HslV are well conserved with those of the prokaryotic HslV. However, a specific interaction between TbHslU2 and TbHslV was detected from the combined structural and biochemical data obtained on TbHslV. Thus, this study lays the groundwork for understanding the eukaryotic HslVU system.

EXPERIMENTAL PROCEDURES

Cloning—The template DNA was a kind gift from Prof. Wang (University of California, San Francisco). The DNA coding for mature TbHslV was amplified by polymerase chain reaction (PCR) with forward and reverse primers containing sites for the restriction enzymes NdeI and XhoI. The PCR product was cloned into the pET-22b(+) vector, and the resultant plasmid had a C-terminal hexahistidine tag and the essential catalytic threonine residue at its N terminus (Thr^1; Fig. 1*A*). EcHslU and SulA were amplified by colony PCR using *E. coli* DH5α. The PCR product of EcHslU was cloned into pET-12a vector by using the NdeI and BamHI restriction enzyme sites, and the resulting construct contained an N-terminal octahistidine tag. The SulA construct was ligated into the pMAL-p4X vector by using the BamHI and HindIII restriction enzyme sites. All mutants, including T1A TbHslV and EcHslU containing the C-terminal sequence of TbHslU2 ($EcHslU_{TbHslU2}$), were generated using the QuikChange® site-directed mutagenesis technique (Stratagene). The subsequently obtained DNA sequences were confirmed by DNA sequencing.

Protein Overexpression and Purification—TbHslV was transformed into BL21(DE3)RIL cells. The transformed cells were cultured in LB medium containing 50 μg/ml ampicillin and 34 μg/ml chloramphenicol at 37 °C until an $A_{600\ nm}$ reading of 0.5 was obtained. Expression was induced by adding isopropyl β-D-thiogalactoside to a final concentration of 1 mM at 16 °C for 24 h. Cells overexpressing TbHslV were harvested by centrifugation, and the pellet was resuspended in 50 mM Tris-HCl (pH 8.0), 100 mM NaCl, and 10% (w/v) glycerol and then subsequently disrupted by ultrasonication. The cell lysate was centrifuged, and the supernatant was applied to a nickel-chelating Sepharose column (GE Healthcare). Further purification was carried out by successive anion exchange (Mono Q™10/100 GL, GE Healthcare) and size exclusion (Superose™ 6 10/300 GL, GE Healthcare) chromatography. Eluents from columns were analyzed by SDS-PAGE and confirmed by N-terminal sequencing. The final protein solution was concentrated to 10 mg/ml in storage buffer (20 mM Tris-HCl (pH 7.7), 300 mM NaCl, 1 mM EDTA, and 1 mM NaN_3). The expression and purification of EcHslV (7), EcHslU (15, 22), and MBP-SulA (33) have been described previously.

Peptide Synthesis—All C-terminal octapeptides were purchased from Anygen Co. Ltd. (Korea). The peptides used are as follows: VDIKKFIL (TbHslU1); IDLAKYIL (TbHslU2); EDLSRFIL (EcHslU); and IDIKKFIL, VDLKKFIL, VDIAKFIL, VDIAKYIL, IDLSRFIL, EDLARFIL, EDLSKFIL, and EDLSRYIL (point mutant peptides are underlined).

Activity Assay—Peptide hydrolysis was assayed using the chromogenic peptide Z-GGL-AMC (Bachem) as a substrate of TbHslV and EcHslV (34). EcHslU and various octapeptides derived from the sequence of the C-terminal segment of EcHslU, TbHslU1, and TbHslU2 were used for HslV activation. The activity assay was conducted at 37 °C using storage buffer containing 7.5% (v/v) dimethylformamide in a total volume of 200 μl, and the release of AMC was monitored as a fluorescence increment at 440 nm (excited at 360 nm) by using a SpectraMax® M5 system (Molecular Devices, Inc.) with a 96-well plate (Corning). For protein substrate degradation, the MBP-SulA was used as described previously (20, 31, 35).

Crystallization and Data Collection—TbHslV was crystallized using the sitting drop or hanging drop vapor diffusion method. In all cases, crystallization was performed at 22 °C. For the hanging drop vapor diffusion method, the crystallization drop comprised 200 nl of protein and an equal volume of reservoir solution containing 0.1 M acetate (pH 5.5), 2.0 M ammonium sulfate, and 2% (w/v) PEG 400. The crystallization set-up was done by using a Mosquito® crystallization robot (TTP LabTech, Melbourn, UK). The crystal was obtained within a day. The Form-I crystal belongs to monoclinic space group $P2_1$ with unit cell parameters of $a = 100.9$ Å, $b = 107.0$ Å, $c = 132.8$ Å, and $\beta = 104.3°$.

For the hanging drop vapor diffusion method, each crystallization drop was mixed with 1 μl of protein and an equal volume of reservoir solution, which contains 0.1 M Tris-HCl (pH 8.5) and 3.5 M sodium formate. Thus, the crystal Form-II was obtained in the orthorhombic space group I222, with cell parameters of $a = 105.9$ Å, $b = 111.5$ Å, $c = 117.2$ Å, and $\alpha = \beta = \gamma = 90°$. The cryosolutions were 0.1 M acetate (pH 5.5), 2.0 M ammonium sulfate, 2% (w/v) PEG 400, and 20% (w/v) glycerol for Form-I crystal and 0.1 M Tris-HCl (pH 8.5) and 4.5 M sodium formate for the Form-II crystal. Before the crystals were cryocooled in liquid nitrogen, they were washed in cryosolutions.

Diffraction data were collected at the BL44XU beamline of Spring-8 (Hyogo, Japan) and the NW12 beamline of the Photon Factory (Tsukuba, Japan) by using an ADSC quantum charge-coupled device detector. A total of 180 images were collected with 1° oscillation, and each image was exposed for 0.8 s. The diffraction data were processed and scaled using the HKL2000 software package (36), and the statistics for the data collection are described in Table 1.

Structure Determination and Refinement—Phases were obtained by molecular replacement with the program MOLREP (37) in the CCP4 program suite (38). A previously determined structure of EcHslV was used as a search model (15). The initial model was rebuilt and refined using standard protocols in COOT (39), PHENIX (40, 41), and REFMAC (42) until the *R*-factor was converged. During the refinement, non-crystallographic symmetry restraints were applied. The refinement statistics for the TbHslV structures are described in Table 1.

TABLE 1
Data collection and refinement statistics

	Form-I	Form-II
Data collection		
X-ray sources[a]	BL44XU, SP8	NW12, PF
Space group	$P2_1$	I222
Cell dimensions		
a, *b*, *c* (Å)	100.88, 106.99, 132.66	105.67, 111.06, 116.95
α, β, γ (degrees)	90.00, 104.24, 90.00	90.00, 90.00, 90.00
No. of subunits/ASU[b]	12	3
Measured reflections	380,128	146,584
Unique reflections	106,506	21,375
Resolution (Å)	2.4 (2.4–2.49)[c]	2.6 (2.6–2.69)
Overall ($I/\sigma I$)	15.6 (3.6)	41.4 (5.7)
R_{sym} (%)[d]	13.3 (48.1)	5.2 (43.6)
R_{meas} or $R_{r.i.m.}$ (%)[e]	15.7 (56.8)	5.6 (47.0)
$R_{p.i.m.}$ (%)[f]	8.2 (30.5)	2.1 (17.7)
Completeness (%)	99.3 (97.4)	99.6 (100)
Redundancy	3.6 (3.3)	6.9 (6.9)
Refinement		
Resolution range (Å)	41.13–2.39	33.73–2.60
Reflections used	100,827	20,054
R_{work}/R_{free} (%)[g]	21.80/23.87	20.97/24.81
No. of atoms	16,562	3,967
Protein residues	2,088	519
Waters	634	31
Average *B* factors (Å^2)		
Main chains	14.56	39.99
Side chains and waters	20.54	47.01
All atoms	17.52	43.34
r.m.s. deviations		
Bond length (Å)	0.016	0.014
Bond angles (degrees)	1.646	1.544
Ramachandran outliers	0	0
Protein Data Bank code	4HNZ	4HO7

[a] SP8, Spring-8 (Japan); PF, Photon Factory (Japan).
[b] ASU, asymmetric unit.
[c] Values in parentheses are for reflections in the highest resolution bin.
[d] $R_{sym} = \Sigma_h\Sigma_i|I(h,i) - \langle I(h)\rangle|/\Sigma_h\Sigma_i I(h,i)$, where $I(h,i)$ is the intensity of the *i*th measurement of reflection *h* and $\langle I(h)\rangle$ is the corresponding average value for all *i* measurements.
[e] $R_{meas} = R_{r.i.m.}$ (redundancy-independent merging *R*-factor) $= \Sigma_h(N/(N-1))^{1/2}\Sigma_i(|I_i(h) - \langle I(h)\rangle|)/\Sigma_h\Sigma_i I_i(h)$.
[f] $R_{p.i.m.}$ (precision-indicating merging *R*-factor) $= \Sigma_h(1/(N-1))^{1/2}\Sigma_i(|I_i(h) - \langle I(h)\langle|)/\Sigma_h\Sigma_i I_i(h)$.
[g] $R_{work} = \Sigma||F_o| - |F_c||/\Sigma|F_o|$, where R_{free} is calculated for the 5% test set of reflections.

Assessment of model geometry and assignment of secondary structural elements were achieved using the program MOLPROBITY (43). Figures depicting molecular structures were generated using CCP4MG (44).

Molecular Modeling—The complex model between TbHslV and the C-terminal segment of TbHslU2 was generated using an HiHslVU complex structure (HslVU complex from *Haemophilus influenzae*) as a template (16). The coordinates of TbHslV are well superposed with those of HslV from *H. influenzae* (HiHslV) in the HiHslVU complex except for the residues from Gly^{48} to Ala^{93}. As a result of this superposition, the structure of TbHslV from residue 48 to 93 was replaced with the structure of HiHslV from the same corresponding residues. The alteration of this structure was then realigned with the sequence of TbHslV. The initial model was energy-minimized with SPBDV (45) and the CNS package (46).

RESULTS

Overproduction and Purification of Mature TbHslV—It is known that one HslV and two HslUs exist in *T. brucei* (28), which have N-terminal signal peptides that direct them to the mitochondria. Excluding the signal sequence, TbHslV shares 41.4% sequence identity with EcHslV and 46.3% sequence identity with HiHslV (Fig. 1*A*). In addition, TbHslU1 and TbHslU2 share 43.0 and 40.6% sequence identity with EcHslU and 43.2 and 41.2% sequence identity with HslU from *H. influenzae* (HiHslU), respectively (28). The mature form, in which the signal sequence (residues 1–19) is removed, has the catalytic threonine residue at the new N terminus; the adjacent residue is also threonine (Fig. 1*A*), which is a distinct feature of N-terminal threonine proteases, including HslV as well as the 20 S proteasome (3, 47). Indeed, there are also tandem threonine residues at the 8th and 9th positions (Fig. 1*A*). Therefore, we generated three different constructs (1-end, 8-end, and 20-end); only the TbHslV construct without the putative N-terminal 19-residue signal sequence was well expressed in *E. coli*, whereas the remaining constructs were expressed at low levels and were insoluble. Similar behavior was observed with full-length HslV from *Thermotoga maritima* (TmHslV), which belongs to the Archaea domain (20). We successfully purified C-terminal His_6-tagged TbHslV, whose sequence begins from the essential catalytic threonine residue. The first methionine was clearly processed. The N-terminal amino acid sequence of purified TbHslV was Thr-Thr-Ile-Ser-Leu, confirmed by the N-terminal sequencing analysis. The oligomeric state of TbHslV is dodecameric in solution, which was confirmed by gel filtration analysis (data not shown). Therefore, the mature form of TbHslV exhibits the basic biochemical characteristics of prokaryotic and archaeal HslVs.

Only the C-terminal Peptide of TbHslU2 Activates the Peptidase Activity of TbHslV—It is known that HslV possesses basically no peptidase and protease activity without its activator HslU (5, 15). For the peptidase activity assay, we tried to overexpress TbHslU1 and TbHslU2 in *E. coli*, but these proteins could not be obtained in soluble form. As an alternative, we checked TbHslV activity in the presence of EcHslU as in the case of CodW, the HslV from *Bacillus* with EcHslU, which shows cross-species reactivity (48). However, we did not observe activation of TbHslV by EcHslU. According to previous reports (8, 16, 30), EDLSRFIL octapeptide, an amino acid sequence derived from the C-terminal 8 residues of EcHslU, can activate EcHslV, as assayed using Z-GGL-AMC as a substrate. Therefore, we synthesized two different octapeptides corresponding to the C-terminal octapeptide regions of TbHslU1 and TbHslU2, respectively (Fig. 1*B*). Unlike the C-terminal peptide of TbHslU1 (VDIKKFIL), only that of TbHslU2 (IDLAKYIL) could activate TbHslV (Fig. 2*A*). In order to check the synergistic activation of TbHslV by both TbHslU1 and TbHslU2 peptides, we measured the activity in the presence of the mixture with both peptides. However, this did not increase the activity of TbHslV, and the level of activation correlated only with the amount of TbHslU2 peptide (Fig. 2*A*). Compared with the activity of EcHslV, that of TbHslV is relatively low. To assess the activity assay result, TbHslV and peptides were set to higher concentration than the established assay conditions with *E. coli* enzymes. This revealed that the octapeptide, IDLAKYIL, which is an amino acid sequence derived from the C-terminal 8 residues of TbHslU2, was an activator of TbHslV activity as assayed with Z-GGL-AMC as substrate. To further confirm the action of TbHslV, we mutated the predicted catalytic threonine residue to alanine (T1A

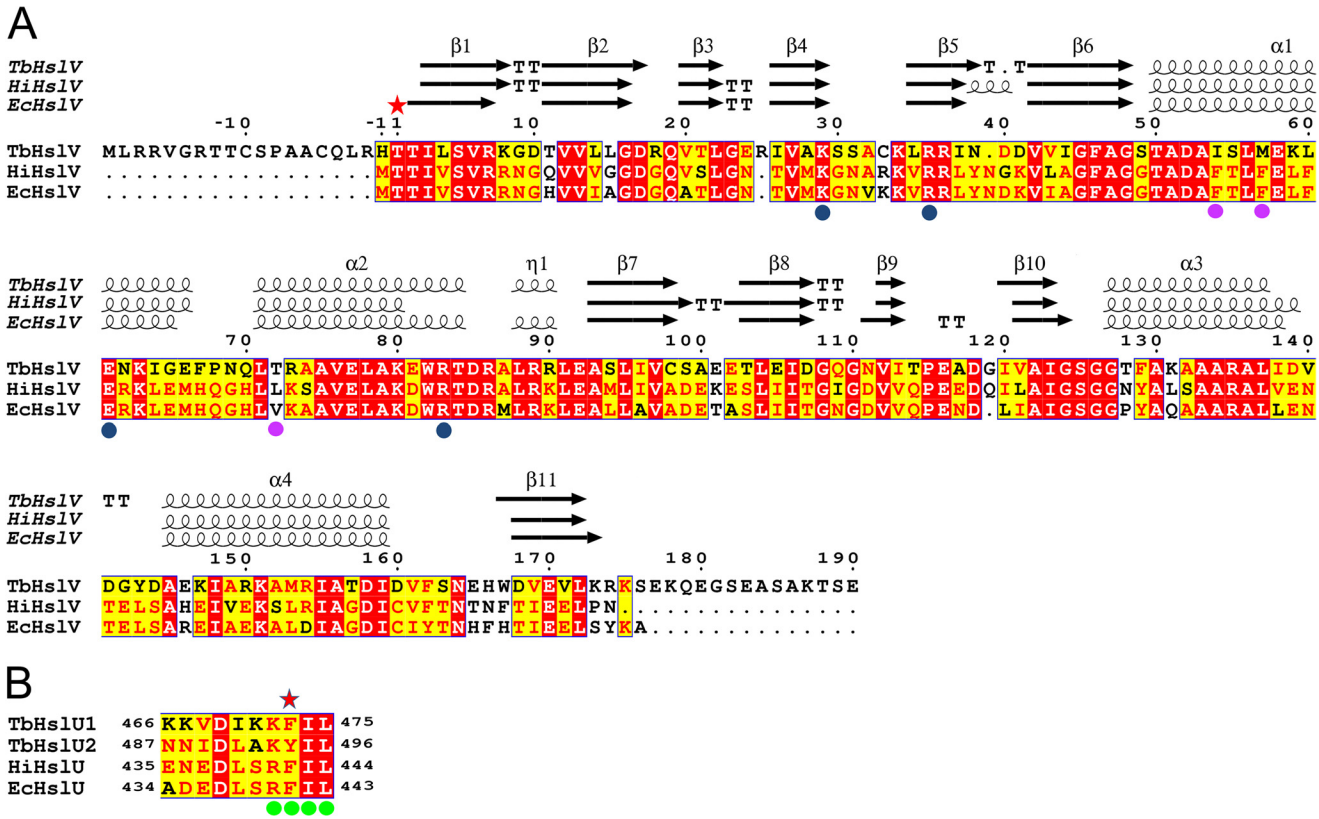

FIGURE 1. **Sequence alignment between HslVs and the C-terminal segment of HslUs.** *A*, sequence alignment of HslV from *T. brucei* (TbHslV; UniProt ID Q383Q5), *H. influenzae* (HiHslV; P43772), and *E. coli* (EcHslV; P0A7B8). Secondary structure elements are indicated *above* the sequence (*spring*, α-helix; *arrow*, β-strand). The *red star* indicates the catalytic threonine (Thr[1]). *Blue circles* indicate residues participating in polar interactions with HslU. Note that the residues marked with *magenta circles* are smaller substitutions that might be important for specific TbHslVTbHslU2 interaction. *B*, sequence alignment of the C-terminal segment in HslU from *T. brucei* (TbHslU1 (UniProt ID Q57VB1) and TbHslU2 (Q382V8)), *H. influenzae* (HiHslU; P43773), and *E. coli* (EcHslU; P0A6H5). The key residue in TbHslU2 for specific interaction with TbHslV is marked with a *red star*. *Green circles* indicate the residues interacting with HslV. *Shading* indicates residues that are identical (*red*) or highly conserved (*yellow*) in all sequences. The sequence number for *T. brucei* enzymes is indicated at the *top* of the alignment in *both panels*.

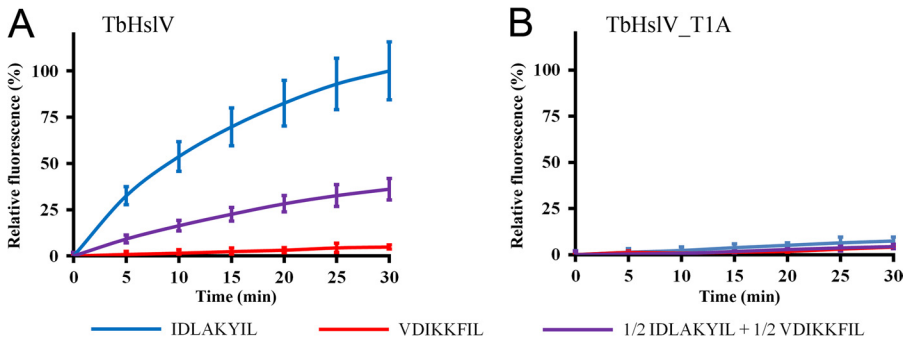

FIGURE 2. **Peptidase activity of TbHslV with the C-terminal peptides of TbHslUs.** Shown is relative activity of wild-type TbHslV (*A*) and T1A mutant enzyme (*B*) with activator peptides. *Blue*, *red*, and *purple lines* represent the activity of TbHslV in the presence of TbHslU2, TbHslU2, and a mixture of equal amounts of both peptides, respectively. The *error bars* were calculated based on three independent experiments. The values are mean ± S.D. ($n = 3$) values.

mutant). As expected, this mutant enzyme does not possess any peptidase activity (Fig. 2*B*).

EcHslU Mutant Mimicking the C-terminal Segment of TbHslU2 Activates TbHslV for Peptide Hydrolysis—As described, EcHslU could not activate TbHslV, whereas the octapeptide IDLAKYIL, derived from the sequence of the C-terminal sequence of TbHslU2, activates the TbHslV. Therefore, we generated an EcHslU mutant containing the C-terminal 8-residue sequence of TbHslU2, termed $EcHslU_{TbHslU2}$. Interestingly, the $EcHslU_{TbHslU2}$ mutant fully activates peptide hydrolysis by TbHslV (Fig. 3*A*). As expected, the activity clearly depends on ATP (Fig. 3*B*).

Next we performed the protein degradation assay in the presence of mutant HslU because folded protein substrates cannot be degraded without the ATPase activity of HslU (31). SulA, a cell division inhibitor in *E. coli*, is encoded by the SOS-inducible *sulA* gene and is a natural substrate of the HslVU complex in *E. coli* (35). The model protein substrate MBP-SulA is recognized by the I-domain of EcHslU and then unfolded and translocated into HslV by the ATPase, HslU (15). As shown in Fig.

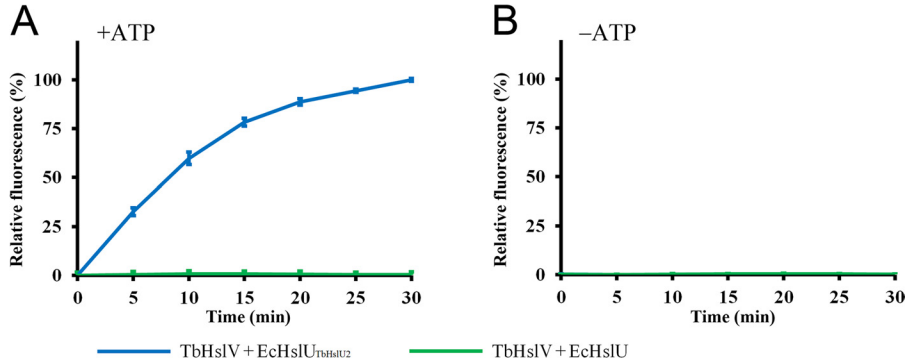

FIGURE 3. **ATP-dependent activity of TbHslV with the mutant HslU protein.** *A*, peptidase activity of TbHslV with the EcHslU$_{TbHslU2}$ mutant. *Blue* and *green lines* represent the activity of TbHslV with EcHslU$_{TbHslU2}$ mutant and EcHslU in the presence of ATP, respectively. *B*, same experiments as those mentioned in *A*, in the absence of ATP. The *error bars* were calculated based on three independent experiments. The values are mean ± S.D. ($n = 3$) values.

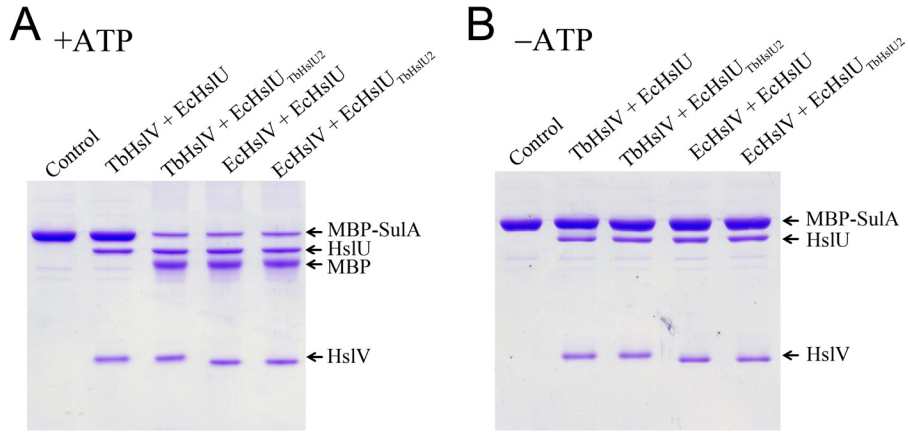

FIGURE 4. **MBP-SulA degradation activity of TbHslV with the EcHslU$_{TbHslU2}$ mutant protein.** *A*, the bands for MBP-SulA (substrate), HslU (EcHslU or EcHslU$_{TbHslU2}$ mutant), MBP (reaction product), and HslV (EcHslV or TbHslV) are indicated. All reactions were performed in the presence of ATP. *B*, same experiments as those mentioned in *A*, in the absence of ATP, which did not yield the product, MBP.

4*A*, the mixture of TbHslV and EcHslU did not trigger degradation of MBP-SulA. However, the mixture between TbHslV and EcHslU$_{TbHslU2}$ hydrolyzed the substrate to a similar extent as the EcHslV-EcHslU complex. Notably, the mixture of EcHslV and EcHslU$_{TbHslU2}$ also hydrolyzed the substrate (Fig. 4*A*, *lane 5*), suggesting that EcHslV is a much more robust protease than TbHslV. No degradation of MBP-SulA substrate was observed in the absence of ATP, confirming that unfolding of the substrate by HslU using ATP energy is a critical step (Fig. 4*B*).

Importance of Tyrosine 494 at the C-terminal Segment of TbHslU2—Next, we analyzed the sequence of the C-terminal residues of TbHslU2. Sequence alignment of the C-terminal segment of several HslUs did not give a clear indication of why only TbHslU2 was capable of activating TbHslV because the sequence at this region is highly homologous (Fig. 1*B*). Therefore, we synthesized various octapeptides and checked the peptidase activity systematically. Because only the peptide comprising the sequences IDLAKYIL (TbHslU2) activates TbHslV, we focused on these residues of TbHslU2 as they differ with those of EcHslU and TbHslU1, which were inactive in the assay. Amino acid residues Asp^{490}, Ile^{495}, and Leu^{496} are strictly conserved in all peptides (all HslUs), whereas Val^{489}, Leu^{491}, Lys^{492}, and Phe^{494} in TbHslU2 are different from corresponding residues in TbHslU1 (Fig. 1*B*). Therefore, we generated four different mutant peptides and checked their ability to activate TbHslV (Fig. 5*A*). Three peptides, IDIKKFIL, VDLKKFIL, and VDIAKFIL (the mutation is underlined for clarity) displayed essentially the same activity as the wild-type TbHslU1 peptide VDIKKFIL (Fig. 5*A*). However, the mutant peptide VDIKK*Y*IL showed significant activation activity.

Four residues in EcHslU (Glu^{436}, Ser^{439}, Arg^{440}, and Phe^{441}) were divergent from those in TbHslU2 (Fig. 1*B*). Three peptides, IDLSRFIL, EDLARFIL, and EDLSKFIL, displayed significantly lower activity than the wild-type EcHslU peptide EDLSRFIL (Fig. 5*A*). The EDLSR*Y*IL mutant fully activated the TbHslV and thus was similar to the TbHslU2 peptide. These data confirm that Tyr^{494} at the C-terminal segment of TbHslU2 is a key residue for TbHslV activation. We performed the same experiments with different enzymatic reaction times and confirmed the results, as shown in Fig. 5, *B* and *C*.

Structure of TbHslV—The crystal structure of TbHslV was solved using the molecular replacement method with EcHslV (Protein Data Bank code 1E94) as the search model (15). The general structural features of TbHslV are well conserved, with a dodecamer of two stacked hexameric rings containing an axial entrance pore (Fig. 6, *A* and *B*), the proteasomal β-subunit folding of its monomer (Fig. 6*C*), and the N-terminal catalytic threonine residue, similar to other HslVs (Fig. 1*A*) (3). The monomeric subunit of TbHslV is composed of four α-helices, 11 β-strands, and connecting loops (Fig. 1*C*). The residues in the monomeric subunit form hydrogen bonds (or salt bridges) with those in the neighboring subunits (Ala^{28m}–Lys^{131n}, Lys^{29}–

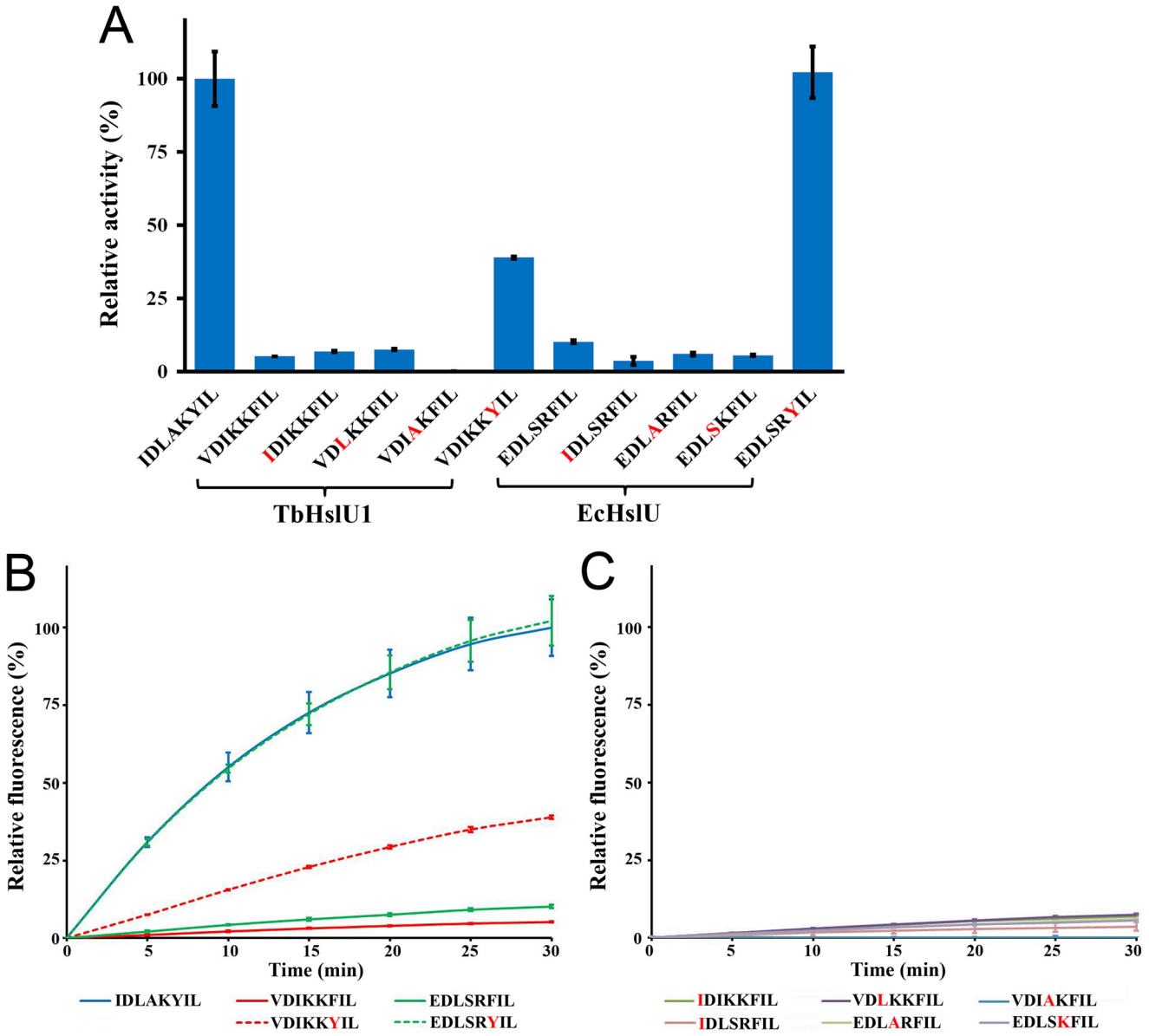

FIGURE 5. **Peptide degradation activity of TbHslV with various point mutants of C-terminal HslU octapeptide.** *A*, relative activity of TbHslV with C-terminal octapeptides of TbHslU1 and EcHslU mutating a residue one by one corresponding to the sequence of TbHslU2. Bar graphs compare the data at a fixed time point (30 min). The mutated residue in each peptide is *highlighted* in *red*. *B* and *C*, kinetic data for the peptide degradation, which also show the importance of the tyrosine residue at the third position from the C terminus of octapeptides. The *error bars* were calculated based on three independent experiments.

Thr^{114nm}, Ser^{30}/Ser^{31}–Glu^{116n}, Ser^{49}–Gln^{109nm}, Asp^{52}–Arg^{83n}, Glu^{58}–Lys^{80n}, Arg^{86}/Arg^{90}–Arg^{86n}, and Arg^{89}–Arg^{90nm}; for clarity, the letter "n", slash, and letter "m" denote the neighboring subunit, bipartite contribution, and main chain atom, respectively) and additional hydrophobic interactions (Ile^{26}–Ile^{159n}, Ala^{28}–Ile^{113n}, and Ala^{51}–Ala^{79n}) for formation of the hexameric rings.

The dodecameric structure of TbHslV is mediated via hexameric ring-ring interactions, which are mainly hydrophobic in nature (Ile^{26}–Phe^{129n}, Thr^{128}–Phe^{129n}, Ala^{132}–Ile^{155n}, and Ala^{136}–Leu^{137n}). Additional polar interactions (Lys^{151}–Ala^{136nm}/Asp^{139n}) contribute to the formation of the dodecamer. These results show that polar interactions, including hydrogen bond and salt bridges, are dominant during formation of the hexameric ring, whereas hydrophobic interactions contribute to the donut shape of the TbHslV dodecamer (Fig. 6*A*). The aforementioned resides are generally well conserved with prokaryotic HslVs (Fig. 1*A*).

Structural Comparison of TbHslV with Other HslVs—The overall structure of TbHslV is similar to that of previously determined HslV structures from prokaryotic species, including *E. coli* (7, 15, 18), *H. influenzae* (16), and *T. maritima* (20). A superimposition of the TbHslV, EcHslV, and HiHslV structures is shown in Fig. 6*B*. The root mean square (r.m.s.) deviation is ~1.4 Å between EcHslV (Protein Data Bank code 1E94) and both crystal forms of TbHslV (Protein Data Bank codes 4HNZ (Form-I) and 4HO7 (Form-II)) with 170 matching C$^{\alpha}$ atoms (residues 1–27, 29–38, 39–118, and 120–172). The r.m.s. deviation is ~1.2 Å between HiHslV (Protein Data Bank code 1G3K) and both TbHslV structures with 171 matching C$^{\alpha}$

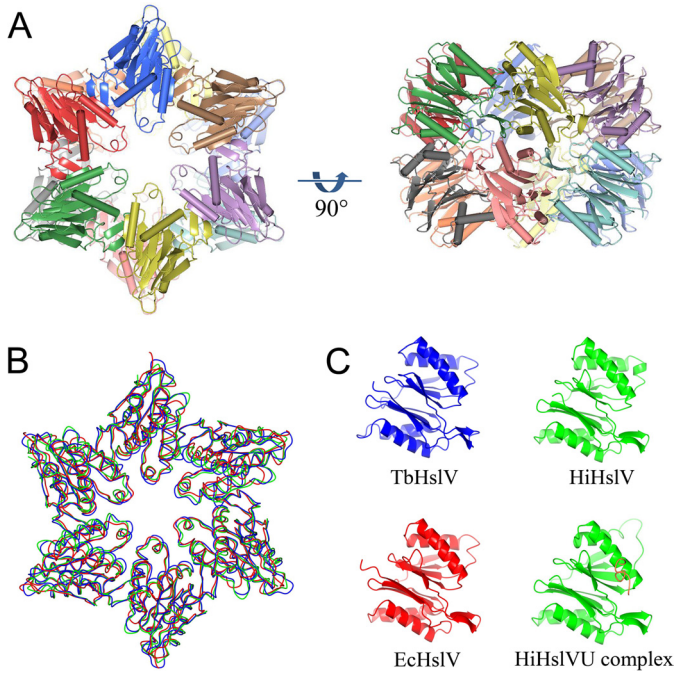

FIGURE 6. **Overall structure of TbHslV and comparison with other HslVs.** A, *ribbon diagram* of dodecameric TbHslV viewed along a 6-fold molecular symmetry axis (*left*). Monomers are *colored differently* for clarity. A *side view* of the TbHslV shows a 2-fold molecule symmetry at the center of the molecule (*right*). *B*, superposition of TbHslV and other HslVs viewed along a 6-fold axis. For clarity, only the upper hexameric ring is shown. The *colors* for each molecule are *blue*, *red*, and *green* for TbHslV, EcHslV, and HiHslV, respectively. *C*, comparison of monomeric subunits among TbHslV, EcHslV, and HiHslV (and HiHslV in complex with HiHslU) *colored* as in *B*. The bound C-terminal segment of HiHslU is shown as a *red trace* (HiHslVU complex).

atoms (residues 1–27, 29–38, and 39–172). The r.m.s. deviations are ~1.3 and 1.4 Å between TmHslV (1M4Y) and Form-I and -II for 170 matching C^{α} atoms (residues 1–27, 29–40, 41–116, and 118–172). Therefore, the overall structural deviations between HslVs are marginal.

An axial entrance pore at the hexameric ring is one of the conserved structural characteristics of HslV (Fig. 6*A*). The entrance pore of TbHslV is a circular shape with a distance of 18.2, 18.5, and 18.5 Å for Form-I and 17.2, 18.7, and 19.0 Å for Form-II, respectively (measuring the distance for three pairs of the C^{α} atom of Arg^{86} on six subunits). The axial entrance pore of TbHslV is slightly smaller than that of other HslVs. The entrance pore size of TmHslV is 19.4, 20.1, and 22.0 Å. However, the entrance pore of the other HslVs has a more elliptical shape with values of 13.1, 19.1, and 25.7 Å for *E. coli* and 13.1, 19.1, and 25.7 Å for *H. influenzae*, respectively. Indeed, the size of entrance pore of HslV also varies upon complex formation with HslU (16, 20) (Fig. 7*A*). Loops with many basic arginine residues in the entrance pore are intrinsically flexible (15, 16). Subsequently, the size of the entrance pore of HslV in the complexed state is greater than that of HslV alone and is mechanistically similar to the entrance pore of the homologous ATP-dependent protease, ClpP (49, 50), and the 20 S proteasome (51, 52).

DISCUSSION

ATP-dependent two-component proteases exist in all three kingdoms of life. The matching symmetry of HslVU consisting of 6-fold HslU ATPase and 6-fold HslV protease is different from that of the eukaryotic 26 S proteasome, which consists of pseudo-6-fold ATPases of the base of the 19 S regulatory particle and 7-fold 20 S proteolytic core. However, the HslV and 20 S proteasome have relatively high structural and sequence similarity, including the same catalytic N-terminal threonine residue (3), suggesting that the HslVU complex is an ancestral type of 26 S proteasome. It has been reported that the HslVU complex only exists in prokaryotes and archaea, whereas the proteasome is present in eukaryotes and archaea (3). In contrast with this hypothesis, the symmetry-mismatched two-component protease ClpXP was identified in chloroplasts and mitochondria of eukaryotes more than 2 decades ago and has been studied extensively (53–56). The coexistence of the HslVU complex and proteasome in eukaryotes has been reported only recently (23, 26–29). The HslVU complex in prokaryotes and archaea possesses a simple architecture consisting of a homododecameric HslV and two homohexameric HslUs, but archaeal and eukaryotic proteasomes display a more complicated configuration. In archaea, several proteasomal ATPases, including proteasome-activating nucleotidase and CDC48, constitute a regulatory network (57), and in eukaryotes, hetero-oligomeric ATPases function within the base of the 19 S regulatory particle. In contrast to prokaryotic and archaeal HslUs, the eukaryotic HslUs from *T. brucei* and *Leishmania donovani* possess two HslU homologs, HslU1 and HslU2 (28, 29); this suggests several possible configurations of the *T. brucei* HslVU complex from a structural point of view: 1) two independent TbHslVU1 and TbHslVU2 complexes; 2) TbHslV asymmetrically capped with hexameric rings of TbHslU1 and TbHslU2, and 3) TbHslV complexed with the hetero-oligomeric TbHslU ring consisting of both TbHslU1 and TbHslU2. The latter case allows for many different combinations, such as different stoichiometries of TbHslU1 and TbHslU2 in the hexameric ring or different symmetries (3-fold, alternative arrangement; 2-fold, three consecutive arrangements) even in the 1:1 composite. As shown in our biochemical data (Fig. 2*A*), the C-terminal segment of TbHslU2 successfully activates TbHslV, whereas that of TbHslU1 does not. Furthermore, TbHslU1 and TbHslU2 do not act synergistically to stimulate the protease activity of TbHslV (Fig. 2*A*). These results rule out the existence of TbHslVU2 and most probably the asymmetrical capped TbHslU1-TbHslV-TbHslU2 complex. Our coexpression experiment of both TbHslU1 and TbHslU2 in *E. coli* did not produce any hetero-oligomers, and more importantly, TbHslV was found to form homo-oligomers and thus possesses all of the same HslU-binding pockets. The TbHslV as well as both TbHslU1 and TbHslU2 are targeted to mitochondria (28); therefore, we speculate that TbHslVU2 and TbHslU1 independently function in regulating mitochondrial DNA.

The reason why only TbHslU2 is able to activate the protease activity of TbHslV remains unclear. TbHslU2 shares high sequence similarity with TbHslU1, as well as with other prokaryotic HslUs (28). Indeed, only the C-terminal segment of HslU participates in binding with HslV (16) and can replace full-length HslU functionally (8, 30). From our biochemical assay, it is evident that Tyr^{494} is a key determinant of HslV activation (Fig. 5*A*). In order to understand the structural basis

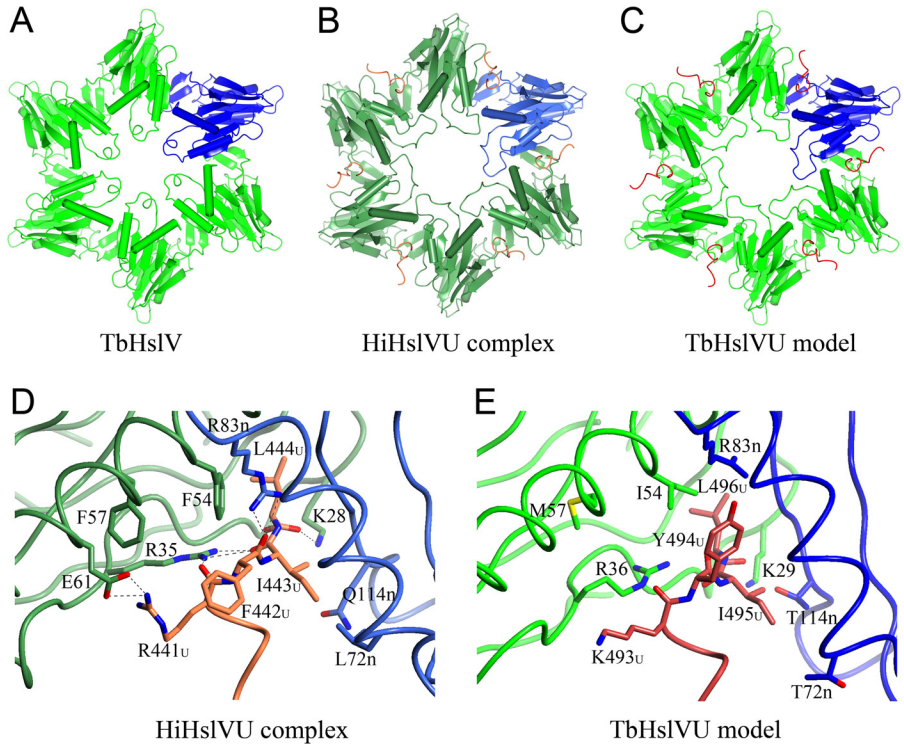

FIGURE 7. **Model of the TbHslV-TbHslU2 complex.** *A*, each monomer in TbHslV is *colored green*, and one monomer is shown in *blue* for clarity. *B*, each monomer in HiHslV is *colored dark green*, and one monomer is shown in *turquoise*. Bound C-terminal segments of HiHslU are *colored orange*. *C*, each monomer in the TbHslVU complex model and the C-terminal segments of TbHslU are *colored red*. *A–C*, the orientation of the model is the same as that in Fig. 6*A*. The loops forming the central pore show different conformations for free and HslU-complexed HslVs. *D*, *close-up view* of the HslU recognition of HiHslV (Protein Data Bank code 1G3K). *E*, same region of the TbHslV model in complex with the TbHslU2 peptide. The *colors* for carbon atoms are the same as in *A–C*. The important residues for the interaction between HslV and HslU are shown as a *stick model* and *labeled*. For clarity, a subscript "U" is added for HslU residues, and a letter *n* is added for adjacent subunits of HslV. Oxygen and nitrogen atoms are *colored red* and *blue*, respectively.

for the activation of TbHslV by TbHslU2, the crystal structure of the TbHslVU2 complex is required. Unfortunately, we were unable to obtain this crystal, but a homology model of TbHslV in complex with TbHslU2 can be built using the only available functional HslVU structure from *H. influenzae* (16). The C-terminal segment of TbHslU2 also shows a high degree of sequence conservation with that of HiHslU (Fig. 1*B*), and the structure of TbHslV is quite similar to that of HiHslV (Fig. 6*B*). Because there is an allosteric conformational change in HslV upon complex formation with HslU (19), we used the HslU-bound HslV as a template for modeling. Therefore, the model of TbHslV complexed with C-terminal segment of TbHslU2 depends on the original complex structure. In particular, the second helix containing Arg^{83}, which participates in salt bridges with the neighboring subunit, shows different structures for apo- and TbHslU2-complexed TbHslV (Fig. 7, *A* and *C*).

In the HiHslVU complex, the Arg^{35} in HiHslV forms hydrogen bonds with the main chain atoms of Arg^{441U} and Ile^{443U} of HiHslU (Fig. 7*D*). For clarity, a "U" is used for the residues of HslU. In addition, Lys^{28} and the adjacent monomer Ala^{83} in HiHslV form hydrogen bonds with the main chain atoms of Leu^{444U} and Phe^{442U} of HiHslU, respectively. Arg^{441U} also forms a salt bridge with Glu^{61}. In addition to the aforementioned interactions, two C-terminal terminal residues, Ile^{443U} and Leu^{444U}, bind tightly to the surrounding hydrophobic residues of HiHslV.

In the TbHslVU complex model, Arg^{36} might form hydrogen bonds with the main chain atoms of Lys^{493U} and Ile^{495U} of TbHslU2 (Fig. 7*E*). The critical residue for TbHslV activation is Tyr^{494U} (Fig. 5*A*), and its equivalent residue in HiHslV is Phe^{442U}. Therefore, the hydroxyl moiety of TbHslU2 must play a critical role in binding. Interestingly, the hydrophobic interaction between TbHslV and TbHslU appears much weaker than that between HiHslV and HiHslV. The residues for accommodating the C-terminal tail of HiHslU, Phe^{54}, Phe^{57}, and Gln^{114n} are replaced with smaller or shorter residues (*i.e.* Ile^{54}, Met^{57}, and Thr^{114n}, respectively) in TbHslV. This explains why EcHslU and TbHslU1 are not able to activate TbHslV, most probably due to the weak binding. Consequently, this replacement with smaller residues may provide space for swinging over the critical tyrosine residue to achieve tighter binding in the TbHslVU2 complex (Fig. 7*E*). Indeed, our modeling study shows that the side chain of Tyr^{494U} could fit into a different rotamer position and that the hydroxyl group forms a hydrogen bond with the main chain atoms of Ala^{79} (Fig. 7*E*). When we analyzed the sequences of several eukaryotic HslUs, many of them were found to have a tyrosine residue at the equivalent position (see the ExPASy Web site). For example, there are two potential HslUs in *L. donovani*, and HslU1 (E9BC50_LEIDB) and HslU2 (E9B9S7_LEIDB) have phenylalanine and tyrosine residues at the critical position, respectively. An HslV ortholog in *Plasmodium falciparum* also has a tyrosine residue at this site (26). Therefore, we infer that the existence of the tyrosine residue in this position can determine the selection of functional HslU molecules in the eukaryotic HslVU system.

Acknowledgments—We thank the staff at the NW12 beamline (Photon Factory) and at the BL44XU beamline (Spring-8, Japan) for help with data collection and C. C. Wang (University of California, San Francisco) for HslV, HslU1, and HslU2 DNAs from T. brucei.

REFERENCES

1. Sauer, R. T., Bolon, D. N., Burton, B. M., Burton, R. E., Flynn, J. M., Grant, R. A., Hersch, G. L., Joshi, S. A., Kenniston, J. A., Levchenko, I., Neher, S. B., Oakes, E. S., Siddiqui, S. M., Wah, D. A., and Baker, T. A. (2004) Sculpting the proteome with AAA+ proteases and disassembly machines. *Cell* **119,** 9–18
2. Baker, T. A., and Sauer, R. T. (2006) ATP-dependent proteases of bacteria. Recognition logic and operating principles. *Trends Biochem. Sci.* **31,** 647–653
3. Bochtler, M., Ditzel, L., Groll, M., Hartmann, C., and Huber, R. (1999) The proteasome. *Annu. Rev. Biophys. Biomol. Struct.* **28,** 295–317
4. Rohrwild, M., Coux, O., Huang, H. C., Moerschell, R. P., Yoo, S. J., Seol, J. H., Chung, C. H., and Goldberg, A. L. (1996) HslV-HslU. A novel ATP-dependent protease complex in *Escherichia coli* related to the eukaryotic proteasome. *Proc. Natl. Acad. Sci. U.S.A.* **93,** 5808–5813
5. Yoo, S. J., Seol, J. H., Shin, D. H., Rohrwild, M., Kang, M.-S., Tanaka, K., Goldberg, A. L., and Chung, C. H. (1996) Purification and characterization of the heat shock proteins HslV and HslU that form a new ATP-dependent protease in *Escherichia coli*. *J. Biol. Chem.* **271,** 14035–14040
6. Rawlings, N. D., Morton, F. R., and Barrett, A. J. (2006) MEROPS. The peptidase database. *Nucleic Acids Res.* **34,** D270–D272
7. Bochtler, M., Ditzel, L., Groll, M., and Huber, R. (1997) Crystal structure of heat shock locus V (HslV) from *Escherichia coli*. *Proc. Natl. Acad. Sci. U.S.A.* **94,** 6070–6074
8. Seong, I. S., Kang, M. S., Choi, M. K., Lee, J. W., Koh, O. J., Wang, J., Eom, S. H., and Chung, C. H. (2002) The C-terminal tails of HslU ATPase act as a molecular switch for activation of HslV peptidase. *J. Biol. Chem.* **277,** 25976–25982
9. Yoo, S. J., Shim, Y. K., Seong, I. S., Seol, J. H., Kang, M. S., and Chung, C. H. (1997) Mutagenesis of two N-terminal Thr and five Ser residues in HslV, the proteolytic component of the ATP-dependent HslVU protease. *FEBS Lett.* **412,** 57–60
10. Yoo, S. J., Seol, J. H., Seong, I. S., Kang, M. S., and Chung, C. H. (1997) ATP binding, but not its hydrolysis, is required for assembly and proteolytic activity of the HslVU protease in *Escherichia coli*. *Biochem. Biophys. Res. Commun.* **238,** 581–585
11. Seol, J. H., Yoo, S. J., Shin, D. H., Shim, Y. K., Kang, M. S., Goldberg, A. L., and Chung, C. H. (1997) The heat-shock protein HslVU from *Escherichia coli* is a protein-activated ATPase as well as an ATP-dependent proteinase. *Eur. J. Biochem.* **247,** 1143–1150
12. Park, E., Rho, Y. M., Koh, O. J., Ahn, S. W., Seong, I. S., Song, J. J., Bang, O., Seol, J. H., Wang, J., Eom, S. H., and Chung, C. H. (2005) Role of the GYVG pore motif of HslU ATPase in protein unfolding and translocation for degradation by HslV peptidase. *J. Biol. Chem.* **280,** 22892–22898
13. Park, E., Lee, J. W., Eom, S. H., Seol, J. H., and Chung, C. H. (2008) Binding of MG132 or deletion of the Thr active sites in HslV subunits increases the affinity of HslV protease for HslU ATPase and makes this interaction nucleotide-independent. *J. Biol. Chem.* **283,** 33258–33266
14. Rohrwild, M., Pfeifer, G., Santarius, U., Müller, S. A., Huang, H. C., Engel, A., Baumeister, W., and Goldberg, A. L. (1997) The ATP-dependent HslVU protease from *Escherichia coli* is a four-ring structure resembling the proteasome. *Nat. Struct. Biol.* **4,** 133–139
15. Song, H. K., Hartmann, C., Ramachandran, R., Bochtler, M., Behrendt, R., Moroder, L., and Huber, R. (2000) Mutational studies on HslU and its docking mode with HslV. *Proc. Natl. Acad. Sci. U.S.A.* **97,** 14103–14108
16. Sousa, M. C., Trame, C. B., Tsuruta, H., Wilbanks, S. M., Reddy, V. S., and McKay, D. B. (2000) Crystal and solution structures of an HslUV protease-chaperone complex. *Cell* **103,** 633–643
17. Wang, J., Song, J. J., Seong, I. S., Franklin, M. C., Kamtekar, S., Eom, S. H., and Chung, C. H. (2001) Nucleotide-dependent conformational changes in a protease-associated ATPase HslU. *Structure* **9,** 1107–1116
18. Wang, J., Song, J. J., Franklin, M. C., Kamtekar, S., Im, Y. J., Rho, S. H., Seong, I. S., Lee, C. S., Chung, C. H., and Eom, S. H. (2001) Crystal structures of the HslVU peptidase-ATPase complex reveal an ATP-dependent proteolysis mechanism. *Structure* **9,** 177–184
19. Sousa, M. C., Kessler, B. M., Overkleeft, H. S., and McKay, D. B. (2002) Crystal structure of HslUV complexed with a vinyl sulfone inhibitor. Corroboration of a proposed mechanism of allosteric activation of HslV by HslU. *J. Mol. Biol.* **318,** 779–785
20. Song, H. K., Bochtler, M., Azim, M. K., Hartmann, C., Huber, R., and Ramachandran, R. (2003) Isolation and characterization of the prokaryotic proteasome homolog HslVU (ClpQY) from *Thermotoga maritima* and the crystal structure of HslV. *Biophys. Chem.* **100,** 437–452
21. Kwon, A.-R., Kessler, B. M., Overkleeft, H. S., and McKay, D. B. (2003) Structure and reactivity of an asymmetric complex between HslV and I-domain deleted HslU, a prokaryotic homolog of the eukaryotic proteasome. *J. Mol. Biol.* **330,** 185–195
22. Bochtler, M., Hartmann, C., Song, H. K., Bourenkov, G. P., Bartunik, H. D., and Huber, R. (2000) The structures of HslU and the ATP-dependent protease HslU-HslV. *Nature* **403,** 800–805
23. Ruiz-González, M. X., and Marín, I. (2006) Proteasome-related HslU and HslV genes typical of eubacteria are widespread in eukaryotes. *J. Mol. Evol.* **63,** 504–512
24. Couvreur, B., Wattiez, R., Bollen, A., Falmagne, P., Le Ray, D., and Dujardin, J.-C. (2002) Eubacterial HslV and HslU subunits homologs in primordial eukaryotes. *Mol. Biol. Evol.* **19,** 2110–2117
25. Gille, C., Goede, A., Schlöetelburg, C., Preissner, R., Kloetzel, P.-M., Göbel, U. B., and Frömmel, C. (2003) A comprehensive view on proteasomal sequences. Implications for the evolution of the proteasome. *J. Mol. Biol.* **326,** 1437–1448
26. Tschan, S., Kreidenweiss, A., Stierhof, Y.-D., Sessler, N., Fendel, R., and Mordmüller, B. (2010) Mitochondrial localization of the threonine peptidase PfHslV, a ClpQ ortholog in *Plasmodium falciparum*. *Int. J. Parasitol.* **40,** 1517–1523
27. Barboza, N. R., Cardoso, J., de Paula Lima, C. V., Soares, M. J., Gradia, D. F., Hangai, N. S., Bahia, M. T., de Lana, M., Krieger, M. A., and Guerra de Sá, R. (2012) Expression profile and subcellular localization of HslV, the proteasome related protease from *Trypanosoma cruzi*. *Exp. Parasitol.* **130,** 171–177
28. Li, Z., Lindsay, M. E., Motyka, S. A., Englund, P. T., and Wang, C. C. (2008) Identification of a bacterial-like HslVU protease in the mitochondria of *Trypanosoma brucei* and its role in mitochondrial DNA replication. *PLoS Pathog.* **4,** e1000048
29. Chrobak, M., Förster, S., Meisel, S., Pfefferkorn, R., Förster, F., and Clos, J. (2012) *Leishmania donovani* HslV does not interact stably with HslU proteins. *Int. J. Parasitol.* **42,** 329–339
30. Ramachandran, R., Hartmann, C., Song, H. K., Huber, R., and Bochtler, M. (2002) Functional interactions of HslV (ClpQ) with the ATPase HslU (ClpY). *Proc. Natl. Acad. Sci. U.S.A.* **99,** 7396–7401
31. Seong, I. S., Oh, J. Y., Yoo, S. J., Seol, J. H., and Chung, C. H. (1999) ATP-dependent degradation of SulA, a cell division inhibitor, by the HslVU protease in *Escherichia coli*. *FEBS Lett.* **456,** 211–214
32. Kanemori, M., Yanagi, H., and Yura, T. (1999) The ATP-dependent HslVU/ClpQY protease participates in turnover of cell division inhibitor SulA in *Escherichia coli*. *J. Bacteriol.* **181,** 3674–3680
33. Sonezaki, S., Ishii, Y., Okita, K., Sugino, T., Kondo, A., and Kato, Y. (1995) Overproduction and purification of SulA fusion protein in *Escherichia coli* and its degradation by Lon protease *in vitro*. *Appl. Microbiol. Biotechnol.* **43,** 304–309
34. Kanaoka, Y. (1985) New fluorogenic substrates for subtilisin. *Chem. Pharm. Bull.* **33,** 1721–1724
35. Higashitani, A., Ishii, Y., Kato, Y., and Koriuchi, K. (1997) Functional dissection of a cell-division inhibitor, SulA, of *Escherichia coli* and its negative regulation by Lon. *Mol. Gen. Genet.* **254,** 351–357
36. Minor, W., Tomchick, D., and Otwinowski, Z. (2000) Strategies for macromolecular synchrotron crystallography. *Structure* **8,** R105–R110
37. Vagin, A., and Teplyakov, A. (2010) Molecular replacement with MOLREP. *Acta Crystallogr. D Biol. Crystallogr.* **66,** 22–25
38. Winn, M. D., Ballard, C. C., Cowtan, K. D., Dodson, E. J., Emsley, P., Evans,

P. R., Keegan, R. M., Krissinel, E. B., Leslie, A. G., McCoy, A., McNicholas, S. J., Murshudov, G. N., Pannu, N. S., Potterton, E. A., Powell, H. R., Read, R. J., Vagin, A., and Wilson, K. S. (2011) Overview of the CCP4 suite and current developments. *Acta Crystallogr. D Biol. Crystallogr.* **67,** 235–242
39. Emsley, P., Lohkamp, B., Scott, W. G., and Cowtan, K. (2010) Features and development of Coot. *Acta Crystallogr. D Biol. Crystallogr.* **66,** 486–501
40. Adams, P. D., Afonine, P. V., Bunkóczi, G., Chen, V. B., Davis, I. W., Echols, N., Headd, J. J., Hung, L.-W., Kapral, G. J., Grosse-Kunstleve, R. W., McCoy, A. J., Moriarty, N. W., Oeffner, R., Read, R. J., Richardson, D. C., Richardson, J. S., Terwilliger, T. C., and Zwart, P. H. (2010) PHENIX: a comprehensive Python-based system for macromolecular structure solution. *Acta Crystallogr. D Biol. Crystallogr.* **66,** 213–221
41. Afonine, P. V., Grosse-Kunstleve, R. W., Echols, N., Headd, J. J., Moriarty, N. W., Mustyakimov, M., Terwilliger, T. C., Urzhumtsev, A., Zwart, P. H., and Adams, P. D. (2012) Towards automated crystallographic structure refinement with phenix.refine. *Acta Crystallogr. D Biol. Crystallogr.* **68,** 352–367
42. Murshudov, G. N., Skubák, P., Lebedev, A. A., Pannu, N. S., Steiner, R. A., Nicholls, R. A., Winn, M. D., Long, F., and Vagin, A. A. (2011) REFMAC5 for the refinement of macromolecular crystal structures. *Acta Crystallogr. D Biol. Crystallogr.* **67,** 355–367
43. Chen, V. B., Arendall, W. B., 3rd, Headd, J. J., Keedy, D. A., Immormino, R. M., Kapral, G. J., Murray, L. W., Richardson, J. S., and Richardson, D. C. (2010) MolProbity. All-atom structure validation for macromolecular crystallography. *Acta Crystallogr. D Biol. Crystallogr.* **66,** 12–21
44. McNicholas, S., Potterton, E., Wilson, K. S., and Noble, M. E. (2011) Presenting your structures. The CCP4mg molecular-graphics software. *Acta Crystallogr. D Biol. Crystallogr.* **67,** 386–394
45. Guex, N., Peitsch, M. C., and Schwede, T. (2009) Automated comparative protein structure modeling with SWISS-MODEL and Swiss-PdbViewer. A historical perspective. *Electrophoresis* **30,** S162-S173
46. Brunger, A. T. (2007) Version 1.2 of the crystallography and NMR system. *Nat. Protoc.* **2,** 2728–2733
47. Groll, M., Ditzel, L., Löwe, J., Stock, D., Bochtler, M., Bartunik, H. D., and Huber, R. (1997) Structure of 20S proteasome from yeast at 2.4 Å resolution. *Nature* **386,** 463–471
48. Kang, M. S., Lim, B. K., Seong, I. S., Seol, J. H., Tanahashi, N., Tanaka, K., and Chung, C. H. (2001) The ATP-dependent CodWX (HslVU) protease in *Bacillus subtilis* is an N-terminal serine protease. *EMBO J.* **20,** 734–742
49. Lee, B.-G., Park, E. Y., Lee, K.-E., Jeon, H., Sung, K. H., Paulsen, H., Rübsamen-Schaeff, H., Brötz-Oesterhelt, H., and Song, H. K. (2010) Structures of ClpP in complex with acyldepsipeptide antibiotics reveal its activation mechanism. *Nat. Struct. Mol. Biol.* **17,** 471–478
50. Lee, B. G., Kim, M. K., and Song, H. K. (2011) Structural insights into the conformational diversity of ClpP from *Bacillus subtilis*. *Mol. Cells* **32,** 589–595
51. Groll, M., Bajorek, M., Köhler, A., Moroder, L., Rubin, D. M., Huber, R., Glickman, M. H., and Finley, D. (2000) A gated channel into the proteasome core particle. *Nat. Struct. Biol.* **7,** 1062–1067
52. Rabl, J., Smith, D. M., Yu, Y., Chang, S. C., Goldberg, A. L., and Cheng, Y. (2008) Mechanism of gate opening in the 20S proteasome by the proteasomal ATPases. *Mol. Cell* **30,** 360–368
53. Adam, Z., Rudella, A., and van Wijk, K. J. (2006) Recent advances in the study of Clp, FtsH and other proteases located in chloroplasts. *Curr. Opin. Plant Biol.* **9,** 234–240
54. Halperin, T., Zheng, B., Itzhaki, H., Clarke, A. K., and Adam, Z. (2001) Plant mitochondria contain proteolytic and regulatory subunits of the ATP-dependent Clp protease. *Plant Mol. Biol.* **45,** 461–468
55. Kang, S. G., Ortega, J., Singh, S. K., Wang, N., Huang, N. N., Steven, A. C., and Maurizi, M. R. (2002) Functional proteolytic complexes of the human mitochondrial ATP-dependent protease, hClpXP. *J. Biol. Chem.* **277,** 21095–21102
56. Maurizi, M. R., Clark, W. P., Kim, S. H., and Gottesman, S. (1990) Clp P represents a unique family of serine proteases. *J. Biol. Chem.* **265,** 12546–12552
57. Forouzan, D., Ammelburg, M., Hobel, C. F., Ströh, L. J., Sessler, N., Martin, J., and Lupas, A. N. (2012) The archaeal proteasome is regulated by a network of AAA ATPases. *J. Biol. Chem.* **287,** 39254–39262